
MVAR: Visual Autoregressive Modeling with Scale and Spatial Markovian Conditioning

Jinhua Zhang Wei Long Minghao Han Weiyi You Shuhang Gu*

University of Electronic Science and Technology of China

{jinhua.zjh, shuhanggu}@gmail.com

Codes and models: <https://github.com/LabShuHangGU/MVAR>

Abstract

Essential to visual generation is efficient modeling of visual data priors. Conventional next-token prediction methods define the process as learning the conditional probability distribution of successive tokens. Recently, next-scale prediction methods redefine the process to learn the distribution over multi-scale representations, significantly reducing generation latency. However, these methods condition each scale on all previous scales and require each token to consider all preceding tokens, exhibiting scale and spatial redundancy. To better model the distribution by mitigating redundancy, we propose **Markovian Visual AutoRegressive modeling (MVAR)**, a novel autoregressive framework that introduces scale and spatial Markov assumptions to reduce the complexity of conditional probability modeling. Specifically, we introduce a scale-Markov trajectory that only takes as input the features of adjacent preceding scale for next-scale prediction, enabling the adoption of a parallel training strategy that significantly reduces GPU memory consumption. Furthermore, we propose spatial-Markov attention, which restricts the attention of each token to a localized neighborhood of size k at corresponding positions on adjacent scales, rather than attending to every token across these scales, for the pursuit of reduced modeling complexity. Building on these improvements, we reduce the computational complexity of attention calculation from $\mathcal{O}(N^2)$ to $\mathcal{O}(Nk)$, enabling training with just eight NVIDIA RTX 4090 GPUs and eliminating the need for KV cache during inference. Extensive experiments on ImageNet demonstrate that MVAR achieves comparable or superior performance with both small model trained from scratch and large fine-tuned models, while reducing the average GPU memory footprint by $3.0\times$.

1 Introduction

Autoregressive (AR) models [7, 27, 36, 44, 47], inspired by the next-token prediction mechanisms of language models, have emerged as a powerful paradigm for modeling visual data priors in image generation tasks. Conventional AR models [7, 50] typically adopt a raster-scan order for conditional probability modeling, which suffers from excessive decoding steps and results in substantial generation latency. To mitigate this latency, pioneering studies have explored modifying token representation patterns [21, 25, 28, 31] or redefining the decoding order [2, 27, 53]. Recently, visual autoregressive modeling (VAR) [46] has shifted visual data priors modeling from next-token prediction to a next-scale prediction paradigm, which sequentially generates multi-scale image tokens in a coarse-to-fine manner. As the next-scale prediction paradigm better preserves the intrinsic two-dimensional structure of images at each scale, VAR improves both the efficiency of the modeling process and the generation quality compared to conventional AR baselines.

*Corresponding author.

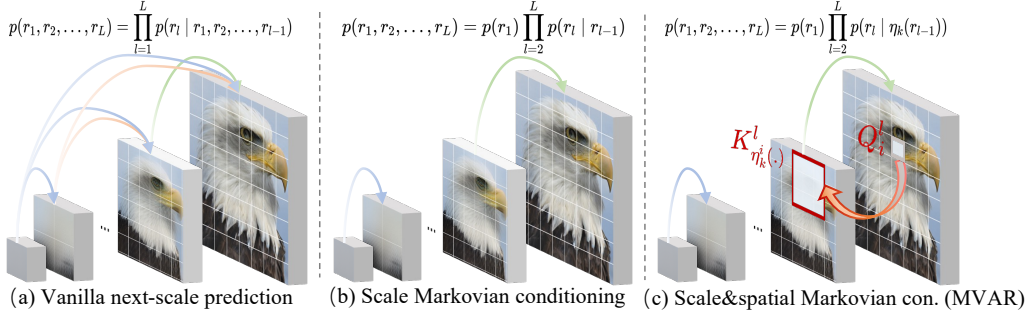


Figure 1: **Vanilla next-scale prediction vs. MVAR.** **Left:** The vanilla next-scale method predicts each scale based on all previous scales and requires each token to consider all preceding tokens. **Middle:** A next-scale variant predicts the next scale using only the adjacent scale, leveraging scale Markovian conditioning across scales. **Right:** MVAR further disentangles the spatial constraint and predicts each token using the neighboring positions of adjacent scales, based on spatial Markovian conditioning.

Although vanilla next-scale prediction methods [4, 12, 45, 46] dramatically accelerate the generation process, our key observations, as shown in Fig. 2 (a) and (b), reveal that approximate conditional independence, both across scales and between adjacent spatial locations, can be further leveraged to mitigate redundancy and improve the generation process. More specifically, vanilla next-scale prediction methods [45, 46] utilize tokens from all preceding scales to predict tokens of next-scale. However, as illustrated in Fig. 2(a), the analysis of attention weights across scales reveals that each scale predominantly relies on its immediately preceding neighbor and is approximately independent of non-adjacent scales. Such cross-scale conditional independence allows us to establish scale-Markov next-scale prediction model for reducing GPU memory consumption and eliminating redundant computation. On the other hand, conventional next-scale prediction methods [45, 46] adopt the features of all preceding tokens as keys and values in attention operations [49]. Nevertheless, as represented in Fig. 2(b), the analysis of accumulated attention weights across adjacent scales with different neighborhood sizes reveals that each token primarily relies on its immediate neighbors rather than all preceding tokens. Such approximate spatial conditional independence makes it possible to further simplify our scale-Markov model with a spatial-Markov constraint.

Building upon the above observations, we introduce scale and spatial Markovian assumptions into the vanilla next-scale prediction model and propose Markovian Visual AutoRegressive (MVAR) model for effective modeling of visual data priors. Instead of relying on all preceding scales to predict the current scale, as shown in Fig. 1(a) for conventional next-scale prediction method [46], we introduce scale-Markov assumption which models the transition probabilities between adjacent scales, as illustrated in Fig. 1(b). This design enables the learning of a scale-Markov trajectory with a parallel training strategy, significantly reducing GPU memory consumption and computational redundancy. In addition to the scale-Markov assumption, we further introduce a spatial-Markov constraint which confines each token’s receptive field to a neighborhood of size k at its corresponding position. As depicted in Fig. 1(c), the proposed spatial-Markov constraint further reduces the computational footprint of our model. Based on the above improvements, MVAR reduces the computational complexity of attention calculation from $\mathcal{O}(N^2)$ to $\mathcal{O}(Nk)$, enables training on eight NVIDIA RTX 4090 GPUs, and eliminates the need for KV cache during inference. Extensive experiments on ImageNet 256×256 demonstrate the advantages of our model. Compared to the vanilla VAR model, our proposed Markovian constraints not only reduce memory and computational footprints for visual modeling, but also improve modeling accuracy by focusing on more important information.

Our main contributions are summarized as follows: **(i)** We propose a novel next-scale autoregressive framework that introduces the scale Markovian assumption to model the conditional likelihood, substantially reducing memory consumption during both training and inference, and enabling the training of MVAR on eight NVIDIA RTX 4090 GPUs. **(ii)** Based on the learned scale-Markov transition probabilities, we introduce spatial-Markov attention to mitigate spatial redundancy across adjacent scales, reducing the computational complexity of attention calculation from $\mathcal{O}(N^2)$ to $\mathcal{O}(Nk)$. **(iii)** We conduct comprehensive experiments on both small model trained from scratch and large fine-tuned models. Our method achieves comparable or superior performance to the vanilla next-scale prediction model while reducing memory consumption by $4.2\times$, as shown in Fig. 2(c).

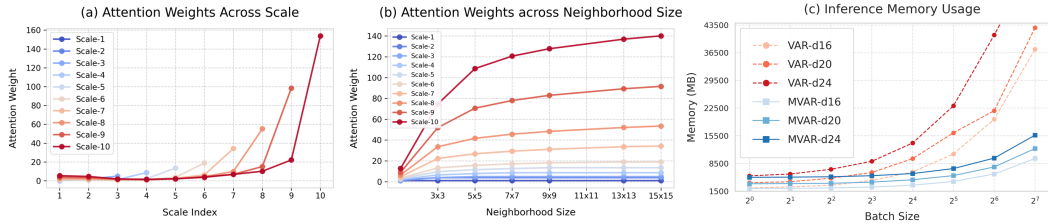


Figure 2: **Left:** Accumulated attention weights across scales in VAR [46]. At each scale, the highest attention weight occurs at the adjacent scale, indicating a predominant focus on neighboring scales rather than all preceding ones. **Middle:** Accumulated attention weights across varying neighborhood sizes between adjacent scales in VAR. As the neighborhood expands, attention weight growth becomes more gradual, indicating a spatially localized focus rather than engagement with all preceding tokens. **Right:** Memory usage during inference. MVAR reduces memory consumption by $4.2 \times$ compared to VAR-d24 (9,860MB vs. 40,971MB at batch size 64) through scale and spatial Markovian conditioning, demonstrating a significant improvement in memory consumption.

2 Related Work

GAN and Diffusion Image Generation methods have been extensively investigated for image synthesis. In contrast to AR models, GANs [8] learn a mapping from a noise distribution to the high-dimensional image space in a single pass via adversarial training, enabling efficient sampling. Pioneering efforts include the LAPGAN [5], which progressively generates images from coarse to fine, and StyleGAN [42], which enables controllable, high-fidelity facial synthesis via unsupervised learning. Further progress has been made by improving architectures [51], training strategies [3], conditioning mechanisms [34], and evaluation metrics [10], advancing both theoretical understanding and practical applications. More recently, unlike the single-step mapping used in GANs, diffusion models decompose image synthesis into a sequence of gradual denoising steps, thereby enabling stable training and improved sample quality. Early methods relied on pixel-space Markovian sampling [17], which incurred high computational cost. Subsequent works improved efficiency through non-Markovian samplers (e.g., DDIM) [43], ODE-based solvers (e.g., DPM-Solver) [29], distillation [41], latent-space sampling (e.g., LDM) [38], and modified architectures [32]. While GANs and diffusion models both yield high-quality images, GANs suffer from training instability, diffusion models offer stability but suffer from slow sampling, and autoregressive models provide strong causal interpretability and support more efficient sampling.

Autoregressive Image Generation methods originate from sequence-prediction tasks in natural language processing. By recursively modeling the conditional probability of each element given all previous ones, these models enable stepwise image synthesis. Early work such as PixelCNN [30] flattened images into one-dimensional pixel sequences and employed gated convolutional layers to capture causal conditional distributions for image synthesis. To overcome the computational bottleneck of next-pixel prediction, VQ-VAE [48] introduced a discrete representation space via a two-stage training process. Subsequently, modeling the next-token distribution in this discrete latent space became the mainstream approach. VQ-GAN [7] further enhanced the discrete representations for next-token prediction by integrating adversarial training and a perceptual loss. MaskGit [2] introduced a bidirectional transformer with random masking that generates multiple discrete tokens in parallel, significantly reducing the number of autoregressive inference steps. More recently, VAR [46] redefined the autoregressive modeling as a next-scale prediction process, mitigating the difficulty of causal modeling. Nonetheless, despite their promising performance, next-scale methods still suffer from excessive memory consumption and high computational costs during training and inference.

3 Methodology

3.1 Preliminary: Autoregressive Modeling via Next-scale Prediction

The conventional next-scale [12, 46] autoregressive modeling introduced by VAR [46] shifts image representation from the raster-scan order token map to multi-scale residual token map, enabling parallel prediction of all token maps at varying scales instead of individual tokens. Following a

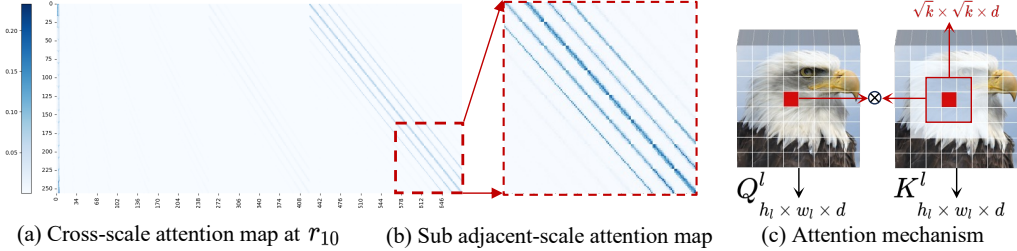


Figure 3: **Attention patterns in the vanilla next-scale prediction method** (e.g., VAR [46]). **Left:** The vanilla next-scale prediction exhibits redundant inter-scale dependencies, as each scale primarily conditions on its adjacent scale rather than all preceding ones. **Middle:** The attention operation between adjacent scales shows spatial redundancy, as each token mostly attends to its immediate spatial neighbors. **Right:** An illustration of the receptive field in the attention mechanism observed in VAR, showing that attention is restricted to local neighborhoods. Additional visual examples are provided in Appendix E.

predefined multi-scale token size sequence $\{(h_l, w_l)\}_{l=1}^L$, it first quantizes the feature map $f \in \mathbb{R}^{h \times w \times C}$ into L multi-scale residual token maps $\mathcal{R} = (r_1, r_2, \dots, r_L)$, each at an increasingly higher resolution $h_l \times w_l$, with r_L matching the resolution of the original feature map $h \times w$. Specifically, the residual token map \hat{r}_l is formulated as:

$$\hat{r}_l = \mathcal{Q}(Down(f - Up(lookup(Z, r_{l-1}), h, w), h_l, w_l)), \quad (1)$$

where $\mathcal{Q}(\cdot)$ is a quantizer, $Down(\cdot, (h_l, w_l))$ and $Up(\cdot, (h, w))$ denote down-sampling or up-sampling a token map to the size (h_l, w_l) or (h, w) respectively, and $lookup(Z, r_l)$ refers to taking the l -th token map from the codebook Z . Then, a standard decoder-only Transformer uses the residual token maps \mathcal{R} to model the autoregressive likelihood:

$$p(r_1, r_2, \dots, r_L) = \prod_{l=1}^L p(r_l | r_1, r_2, \dots, r_{l-1}), \quad (2)$$

where each autoregressive unit r_l is the token map at scale l , containing $h_l \times w_l$ tokens. All previous token maps from r_1 to r_{l-1} , together with the corresponding positional embedding map at scale l , serve as the prefill condition for predicting r_l . During inference, due to the dense inter-scale connections, where r_l is conditioned on all previous token maps, the KV cache must retain the features of all preceding scales to avoid redundant computation.

3.2 Key Observations

In this subsection, we present the motivation behind MVAR based on two key observations from the vanilla next-scale prediction paradigm [46], as revealed by the attention weight analysis in Fig. 2 and the attention map patterns in Fig. 3. First, the attention weights of vanilla next-scale method reveal redundant inter-scale dependencies, leading to excessive GPU memory consumption and computational inefficiency. Second, dense attention operations between adjacent scales display spatial redundancy, where each token primarily attends to its immediate spatial neighbors rather than all preceding tokens, presenting an opportunity to further reduce computational complexity.

Observation 1: Attention weights in vanilla next-scale prediction model exhibit scale redundancy. While vanilla next-scale method utilizes the entire sequence of token maps $(r_1, r_2, \dots, r_{l-1})$ as the conditioning prefix to predict r_l , the information encapsulated in the preceding scale token maps is often redundant for consecutive scale prediction. As demonstrated in Fig. 2(a) and Fig. 3(a), the attention weights across scales reveal that queries at scale l pay negligible attention to all preceding scales, but exhibit a significant concentration on the immediately adjacent scale. This behavior aligns with the hierarchical design, where higher-resolution scales prioritize local refinements rather than reusing features from coarser levels. Consequently, by effectively alleviating such scale redundancy, we can reduce computational complexity and eliminate unnecessary conditioning on earlier scales when predicting next-scale tokens.

Observation 2: Attention weights in vanilla next-scale prediction model exhibit spatial redundancy. Conventional next-scale autoregressive approaches typically utilize Transformer [35] blocks to model

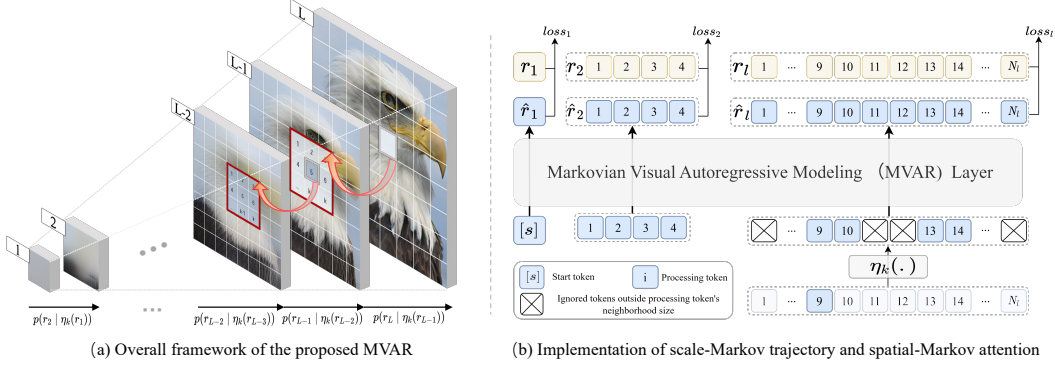


Figure 4: **Overall Framework of MVAR.** First, a scale-Markov trajectory predicts r_l using only its adjacent scale r_{l-1} , discarding all earlier scales. This allows for parallel training across scales using a standard cross-entropy loss $loss_l$. Second, a spatial-Markov attention mechanism restricts attention to a local neighborhood of size k , reducing computational complexity from $\mathcal{O}(N^2)$ to $\mathcal{O}(Nk)$.

transition probabilities. At the core of Transformer is the attention operation, which enhances features by computing weighted sums of token similarities. This operation is formally defined as:

$$Attention(\mathbf{Q}^l, \mathbf{K}^l, \mathbf{V}^l) = \text{SoftMax}\left(\mathbf{Q}^l(\mathbf{K}^l)^T / \sqrt{d}\right) \mathbf{V}^l, \quad (3)$$

where $\mathbf{Q}^l \in \mathbb{R}^{N_l \times d}$, $\mathbf{K}^l \in \mathbb{R}^{N_l \times d}$, and $\mathbf{V}^l \in \mathbb{R}^{N_l \times d}$ are linearly projected from the features of token map r_l , $N_l = h_l \times w_l$ is the token number, and d is feature dimension. While attention operations theoretically enable global context modeling, finer scales which primarily capture textural details exhibit spatial redundancy, such as strong locality and 2D spatial organization, akin to convolutional operations [15]. As depicted in Fig. 3(b), the attention map between adjacent scales exhibits a **diagonally dominant** pattern, indicating that adjacent scales interact predominantly through spatially correlated regions rather than global dispersion. Such geometrically constrained weight distribution mirrors the local connectivity prior inherent in convolutional operations, as illustrated in Fig. 2(b) and Fig. 3(c). As neighborhood size increases, attention distributions become smoother, implying that attention operations across adjacent scales emphasize local textural details over global structural information [4, 11]. Therefore, such spatial redundancy can be leveraged to significantly reduce the $\mathcal{O}(N_l^2)$ time complexity of attention computation, particularly pronounced at finer scales (e.g., r_9 and r_{10}), where attention operations account for up to 60% of the total computational cost.

In summary, the key insights from our observations are as follows: 1) Redundant inter-scale dependencies in hierarchical architectures can be mitigated by introducing the scale-Markovian assumption, which reduces memory usage and enhances computational efficiency. 2) Spatial redundancy in adjacent-scale interactions enables efficient spatial-Markov attention, which approximates localized 2D operations rather than global attention patterns.

3.3 Autoregressive Modeling via Scale and Spatial Markovian Conditioning

To improve the modeling of visual data priors, we introduce MVAR, a novel next-scale autoregressive framework that applies the scale Markovian assumption to inter-scale dependencies and the spatial Markovian assumption to attention across adjacent scales, as illustrated in Fig. 4. In this framework, we restrict inter-scale dependencies to adjacent scales and incorporate localized attention operations into the dense computations between them, reducing memory consumption and computational cost.

Next-scale prediction with scale Markovian conditioning. To better mitigate the observed redundant dependencies across scales, we reformulate autoregressive modeling for next-scale prediction by shifting from the “previous scales-based” [46] paradigm to an “adjacent scale-based” paradigm. Specifically, the conditioning prefix for scale r_l is restricted to its immediate predecessor r_{l-1} , discarding all other preceding scales. Formally, the autoregressive transition probability is defined as:

$$p(r_1, r_2, \dots, r_L) = p(r_1) \prod_{l=2}^L p(r_l | \eta_k(r_{l-1})), \quad (4)$$

where $\eta_k(\cdot)$ restricts attention to preceding tokens within a neighborhood of size k , as discussed below. The term $p(r_1)$ represents the probability distribution of the first scale token, generated from a class embedding referred to as the start token $[s]$. This pruning strategy aligns with the scale redundancy observed in Fig. 2(a) and Fig. 3(a), allowing each scale to focus on local refinements rather than redundantly reusing information from preceding scales.

Attention operation with spatial Markovian conditioning. As illustrated in Fig. 1(b), restricting inter-scale dependencies to adjacent scales reduces redundant interactions; however, dense computations within these adjacent scales remain excessive (see analysis in Fig. 2(b) and attention map patterns in Fig. 3(b)). As shown in Eq. 3, conventional attention operates densely over all tokens in adjacent scales to produce outputs, resulting in quadratic time complexity $\mathcal{O}(N_l^2)$. To mitigate the observed spatial redundancy, we introduce spatial-Markov attention [13, 14], where each query token attends exclusively to its k nearest neighbors, as illustrated in Fig. 4. Specifically, given the query, key, and value matrices $\mathbf{Q}^l \in \mathbb{R}^{N_l \times d}$, $\mathbf{K}^l \in \mathbb{R}^{N_l \times d}$, and $\mathbf{V}^l \in \mathbb{R}^{N_l \times d}$ at scale r_l , we compute the local attention score $\mathbf{S}_i^l \in \mathbb{R}^{1 \times k}$ for the i -th token within a neighborhood of size k as:

$$\mathbf{S}_i^l = \begin{bmatrix} \mathbf{Q}_i^l (\mathbf{K}_{\eta_k^i(1)}^l)^T & \mathbf{Q}_i^l (\mathbf{K}_{\eta_k^i(2)}^l)^T & \cdots & \mathbf{Q}_i^l (\mathbf{K}_{\eta_k^i(k)}^l)^T \end{bmatrix}, \quad (5)$$

where $\eta_k^i(j)$ denotes the index of the j -th neighboring token. Similarly, the local value matrix $\mathbf{V}_i^l \in \mathbb{R}^{k \times d}$ is defined as:

$$\mathbf{V}_i^l = \begin{bmatrix} (\mathbf{V}_{\eta_k^i(1)}^l)^T & (\mathbf{V}_{\eta_k^i(2)}^l)^T & \cdots & (\mathbf{V}_{\eta_k^i(k)}^l)^T \end{bmatrix}^T. \quad (6)$$

Since each token attends only to its k neighboring tokens rather than all tokens as in conventional next-scale paradigms, the computational complexity is reduced from $\mathcal{O}(N_l^2)$ to $\mathcal{O}(N_l k)$. Finally, the spatial-Markov attention output $SA_i^l \in \mathbb{R}^{1 \times d}$ for the i -th token with neighborhood size k is defined as:

$$SA_i^l = \text{SoftMax}(\mathbf{S}_i^l / \sqrt{d}) \mathbf{V}_i^l. \quad (7)$$

Note that during training, by disentangling dependencies between non-adjacent scales such that each r_l only attends to its immediate predecessor r_{l-1} , parallelized training can be adopted on a per-scale basis. Specifically, to maximize GPU utilization, we train scales r_1 through r_8 in parallel using **diagonal pattern** causal masks (more details are provided in Appendix A) that ensure each r_l only attends to its prefix r_{l-1} . During inference, our method eliminates the need for KV cache, thereby further streamlining computational efficiency.

3.4 Analysis of Computational Complexity

Conventional next-scale [46] paradigms incur high computational cost because the number of tokens at each scale equals the sum of tokens from all preceding scales, and dense computation is performed between adjacent scales. In the token generation process of conventional next-scale autoregressive models, the time complexity of producing N tokens is $\mathcal{O}(N^2)$ (see Appendix B for more details), whereas our method reduces this to $\mathcal{O}(Nk)$. Specifically, consider a predefined sequence of multi-scale tokens $\{(h_l, w_l)\}_{l=1}^L$. For simplicity, let $h_l = w_l = \sqrt{N_l}$ for all $1 \leq l \leq L$, and denote $\sqrt{N} = h = w$. We further define $\sqrt{N_l} = a^{l-1}$ for some constant $a > 1$, such that $a^{L-1} = \sqrt{N}$. At the l -th autoregressive generation stage, the total number of tokens is $N_l = a^{2(l-1)}$. Therefore, the time complexity for this stage is $\mathcal{O}(N_l k)$. Summing over all scales yields:

$$\sum_{l=1}^L a^{2(l-1)} k = k \frac{a^{2L} - 1}{a^2 - 1} = k \frac{a^2 N - 1}{a^2 - 1} \sim \mathcal{O}(Nk). \quad (8)$$

4 Experimental Results

In this section, we present the implementation details, report the main results on the ImageNet 256×256 generation benchmark, and conduct ablation studies to evaluate the contribution of each component in our proposed methodology.

Table 1: **Quantitative results on class-conditional ImageNet at resolution 256×256 .** \downarrow / \uparrow indicate that lower / higher values are better. We report results for representative generative models including generative adversarial networks (GANs), diffusion models (DMs), token-wise autoregressive models, and scale-wise autoregressive models. Metrics marked as “–” are not reported in the original papers. VAR [46] is evaluated using the official pretrained weights from its GitHub repository.

Type	Models	FID \downarrow	IS \uparrow	Precision \uparrow	Recall \uparrow	#Params	#Steps
GANs	BigGAN [1]	6.95	224.5	0.89	0.38	112M	1
	GigaGAN [23]	3.45	225.5	0.84	0.61	569M	1
	StyleGAN-XL [42]	2.30	265.1	0.78	0.53	166M	1
DMs	ADM [6]	10.94	101.0	0.69	0.63	554M	250
	CDM [18]	4.88	158.7	–	–	–	8100
	LDM-4-G [39]	3.60	247.7	–	–	400M	250
	Simple-Diffusion [20]	2.44	256.3	–	–	2B	–
	DiT-L/2 [33]	5.02	167.2	0.75	0.57	458M	250
	DiT-XL/2 [33]	2.27	278.2	0.83	0.57	675M	250
Token-wise	MaskGIT [2]	6.18	182.1	0.80	0.51	227M	8
	RCG (cond.) [26]	3.49	215.5	–	–	502M	20
	VQVAE-2 † [37]	31.11	~45	0.36	0.57	13.5B	5120
	VQGAN † [7]	18.65	80.4	0.78	0.26	227M	256
	VQGAN [7]	15.78	74.3	–	–	1.4B	256
	VQGAN-re [7]	5.20	280.3	–	–	1.4B	256
	ViTVQ [52]	4.17	175.1	–	–	1.7B	1024
	ViTVQ-re [52]	3.04	227.4	–	–	1.7B	1024
	DART-AR [9]	3.98	256.8	–	–	812M	–
	RQTran. [25]	7.55	134.0	–	–	3.8B	68
	RQTran.-re [25]	3.80	323.7	–	–	3.8B	68
Scale-wise	VAR [46]	3.55	280.4	0.84	0.51	310M	10
	MVAR	3.09	285.5	0.85	0.51	310M	10

4.1 Implementation Details

We train the 310M model on eight NVIDIA RTX 4090 GPUs with a total batch size of 448 for 300 epochs. For the 600M and larger models, fine-tuning is conducted with a different batch size over 80 epochs. Both models are optimized using the AdamW [24] optimizer with $\beta_1 = 0.9$, $\beta_2 = 0.95$, a weight decay of 0.05, and a base learning rate of 1×10^{-4} . For the predefined multi-scale token length sequence, unless otherwise specified, we adopt the same setting as VAR [46], i.e., $\{1, 2, 3, 4, 5, 6, 8, 10, 13, 16\}$, for the 256×256 resolution. Following common practice, we evaluate Fréchet Inception Distance (FID) [16], Inception Score (IS) [40], Precision, and Recall, along with additional reference metrics. More implementation details are provided in Appendix C.

4.2 Main Results

Overall comparison. We evaluate the performance of our method against the original VAR models [46], conventional next-token prediction models [2, 7, 25, 52], diffusion models [6, 18, 33, 39], and GAN-based approaches [1, 23, 42] on the ImageNet-1K benchmark. As shown in Table 1, our method consistently outperforms nearly all competing models, achieving notable improvements over the VAR baselines. Specifically, compared to VAR, our method reduces the FID by 0.46, and increases the IS by 5.1, demonstrating superior overall performance. As illustrated in Fig. 5, our MVAR produces high-quality images for class-conditional generation on ImageNet 256×256 . Additional qualitative results can be found in Appendix E.

Pre-trained vs. Fine-tuning. To further demonstrate the scale and spatial redundancy observed in conventional next-scale prediction methods, we use pre-trained VAR models as baselines and then fine-tune them, achieving comparable performance with lower GPU memory consumption and computational costs. Specifically, as shown in Table 2, the fine-tuned VAR model not only achieves significant performance improvements over the original model but also attains an average $3.0 \times$

Table 2: **Pre-trained vs. Fine-tuning Comparison.** Quantitative comparison between pre-trained VAR [46] baselines and our fine-tuned variants (MVAR †). Metrics include inference time (seconds per batch), GFLOPs in attention blocks, KV cache footprint (MB), GPU memory usage (MB), training speed (seconds per iteration), and training memory consumption (MB). All experiments were conducted on NVIDIA RTX 4090 GPU with batch size 32. OOM denotes out of GPU memory.

Methods	Time (s) \downarrow	GFLOPs \downarrow	KV Cache \downarrow	Memory \downarrow	Train Speed \downarrow	Train Memory \downarrow	FID \downarrow	IS \uparrow	Precision \uparrow	Recall \uparrow
VAR- $d16$	0.34	43.61	5440M	10882M	0.99	34319M	3.55	280.4	0.84	0.51
MVAR- $d16^{\dagger}$	0.27	35.44	0	3846M (2.8 \times)	0.61 (1.6 \times)	20676M	3.40	297.2	0.86	0.48
VAR- $d20$	0.52	81.52	8500M	16244M	1.35	48173M	2.95	302.6	0.83	0.56
MVAR- $d20^{\dagger}$	0.45	68.75	0	5432M (3.0 \times)	0.79 (1.7 \times)	27665M	2.87	295.3	0.86	0.52
VAR- $d24$	0.81	136.63	12240M	23056M	—	OOM	2.33	312.9	0.82	0.59
MVAR- $d24^{\dagger}$	0.71	118.25	0	7216M (3.2 \times)	0.91	38579M	2.23	300.1	0.85	0.56



Figure 5: **Qualitative results.** Examples of class-conditional generation on ImageNet 256 \times 256.

reduction in inference memory consumption. These results highlight that our approach outperforms the next-scale paradigm, underscoring the benefits of scale and spatial Markovian conditioning.

4.3 Ablation Study

To assess the effectiveness of the core components in our method, we conduct ablation studies focusing on two key aspects: scale Markovian conditioning across scales and spatial Markovian conditioning across adjacent locations. Due to limited computational resources, all results are reported using the 310M model trained under a shorter schedule of 50 epochs.

Effects of scale and spatial Markovian conditioning. To assess the impact of key components in MVAR, we design three model variants and compare their performance, as illustrated in Fig. 6. Method (a) serves as the baseline following the VAR [46] setup. To reveal the redundancy of inter-scale dependencies in this setting, Method (b) uses only the immediate predecessor to model transition probabilities, rather than relying on all preceding non-adjacent scales. Method (c) further introduces spatial-Markov attention, refining the attention mechanism to more effectively capture local textural details. As shown in Fig. 6, even when the strong scale and spatial dependencies are removed, the progressive generation process remains analogous to the conventional next-scale prediction method. Moreover, the combined application of scale-Markov trajectory and spatial-Markov attention achieves improvements across most metrics, notably reducing FID by 0.68, increasing IS by 13.7, and lowering GFLOPs of attention operations by 8.17.

Effects of varying the number of scales in the conditioning prefix. We conduct experiments to investigate the impact of different strategies for modeling inter-scale dependencies. Method (a) follows the original VAR [46] setup and serves as the baseline. Methods (b) and (c) explore limiting the conditioning prefix to only the two or three most recent preceding scales. As shown in Table 3, reducing redundant dependencies leads to lower memory consumption and computational

Table 3: **Ablation study on the number of preceding scales.** Reducing the number of preceding scales decreases memory usage and improves computational efficiency. “(a)” denotes the baseline configuration following the VAR [46] setup. All experiments used an RTX 4090 with batch size 32.

Method	Number	Memory \downarrow	KV Cache \downarrow	Time (s) \downarrow	GFLOPs \downarrow	FID \downarrow	IS \uparrow	Precision \uparrow	Recall \uparrow
(a)	–	10882M	5704M	0.34	43.61	4.84	227.1	0.85	0.43
(b)	3	9518M	3565M	0.32	41.54	4.86	220.3	0.86	0.43
(c)	2	9262M	2147M	0.31	40.15	5.01	208.8	0.84	0.45
(d)	1	4199M (2.6 \times)	0	0.29	37.84	4.35	240.6	0.86	0.45

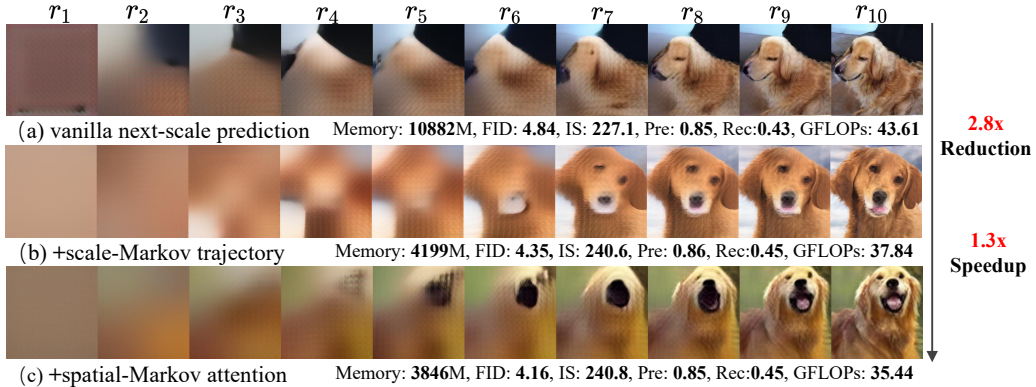


Figure 6: **Ablation study on scale and spatial Markovian conditioning.** Intermediate outputs at scales r_1 to r_{10} illustrating the progressive emergence of semantic and spatial details, along with memory usage and evaluation metrics including FID, IS, Precision (Pre), Recall (Rec), and attention GFLOPs. All experiments were conducted on an NVIDIA RTX 4090 with batch size 32.

cost. Notably, Method (d), which conditions solely on the immediate predecessor, removes the need for KV cache, improves IS by 13.5, and reduces memory usage by 2.6 \times . These results suggest that minimizing inter-scale dependencies helps the model concentrate on essential generative patterns rather than redundant historical information, thereby enhancing generation quality.

Effects of neighborhood size k in spatial-Markov attention. The neighborhood size k is crucial in spatial-Markov attention, as it determines the size of the receptive field. A larger neighborhood provides broader context, generally improving performance. We conduct experiments to examine the effect of varying k from 3×3 to 9×9 , as shown in Table 4. The model improves significantly when k increases to 7×7 , but further increases results in only marginal gains. This is because spatial-Markov attention effectively captures fine-grained details within a compact neighborhood, while larger k values bring diminishing returns and redundant computation, as illustrated in Fig. 2(b). To strike a balance between performance and computational cost, we choose $k = 7 \times 7$ for our final models.

Table 4: **Ablation study on neighborhood size k in spatial-Markov attention.** “–” denotes the baseline configuration following the VAR [46] setup.

k	FID \downarrow	IS \uparrow	Precision \uparrow	Recall \uparrow	GFLOPs \downarrow
–	4.84	227.1	0.85	0.43	43.61
3×3	4.64	243.9	0.85	0.44	34.89
5×5	4.36	235.8	0.86	0.43	35.11
7×7	4.16	240.8	0.85	0.45	35.44
9×9	4.18	237.4	0.85	0.46	35.89

5 Conclusion

In this paper, we propose MVAR, a novel next-scale prediction autoregressive framework that significantly reduces GPU memory usage during training and inference while maintaining superior performance. We introduce the scale-Markov trajectory, which models the autoregressive likelihood using only adjacent scales and discards non-adjacent ones. This design enables parallel training and substantially lowers GPU memory consumption. Furthermore, to address spatial redundancy in attention across adjacent scales, we propose spatial-Markov attention, which restricts attention to a neighborhood of size k , reducing computational complexity of attention calculation from $\mathcal{O}(N^2)$ to $\mathcal{O}(Nk)$. Extensive experiments demonstrate that our method achieves comparable or better performance than existing approaches while significantly reducing average GPU memory usage.

A Schematic of the Scale-wise Causal Mask

In Fig. 7, we show the causal mask used in VAR [46] to model next-scale autoregressive likelihood, which restricts each token r_k to attend only to preceding scales $r_{<k}$. Notably, MVAR employs a **diagonal-pattern mask** that allows each r_k to access only r_{k-1} for the first eight scales ($r_{\leq 8}$). For the final two scales, accounting for 60% of the total tokens, we disable causal masking because these stages use single-scale conditioning to model $p(r_l | \eta_k(r_{l-1}))$.

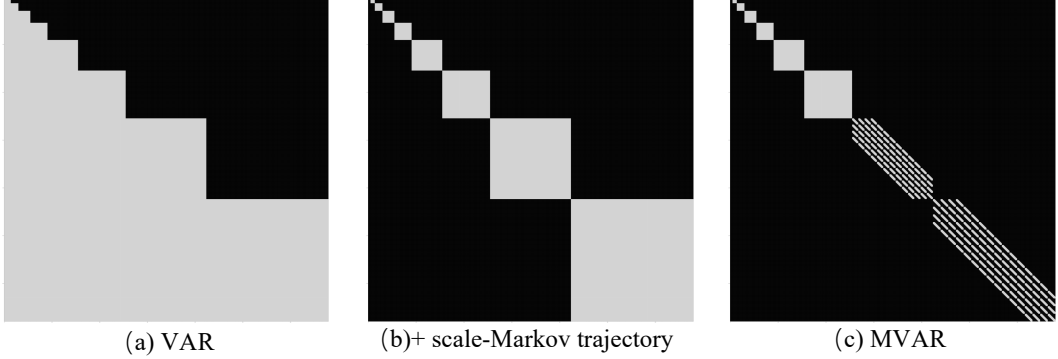


Figure 7: **Schematic of causal masks.** VAR [46] employs a full causal mask to model $p(r_l | r_{<l})$. In MVAR, scales r_1 to r_8 use a **diagonal-pattern mask** to model $p(r_l | r_{l-1})$, since the receptive field is smaller than the neighborhood size k . Scales r_9 and r_{10} are generated without any causal masking to model $p(r_l | \eta_k(r_{l-1}))$.

B Time Complexity Analysis of Different Autoregressive Models

In this section, we demonstrate that the time complexities of conventional next-token prediction methods and vanilla next-scale prediction methods [46] are $\mathcal{O}(N^3)$ and $\mathcal{O}(N^2)$, respectively. In contrast, our MVAR method achieves a time complexity of $\mathcal{O}(Nk)$, as established in Section 3.4.

Consider a **standard next-token prediction** using a self-attention transformer, where the total number of tokens is $N = h \times w$. At generation step i ($1 \leq i \leq N$), the model computes attention scores between the current token and all previous $i-1$ tokens. This operation necessitates $\mathcal{O}(i^2)$ time due to the quadratic complexity of self-attention at each step. Consequently, the overall time complexity is given by

$$\sum_{i=1}^N i^2 = \frac{1}{6} N(N+1)(2N+1) \sim \mathcal{O}(N^3). \quad (9)$$

On the other hand, consider a predefined multi-scale length $\{(h_l, w_l)\}_{l=1}^L$. For simplicity, let $h_l = w_l = \sqrt{N_l}$ for all $1 \leq l \leq L$, and denote $\sqrt{N} = h = w$. We further define $\sqrt{N_l} = a^{l-1}$ for some constant $a > 1$ such that $a^{L-1} = \sqrt{N}$. For **vanilla next-scale prediction**, at the l -th scale generation stage, the total number of tokens can be expressed as

$$\sum_{i=1}^l N_i = \sum_{i=1}^l a^{2(i-1)} = \frac{a^{2l} - 1}{a^2 - 1}. \quad (10)$$

Thus, the time complexity for the l -th scale generation process is $\left(\frac{a^{2l} - 1}{a^2 - 1}\right)^2$. By summing across all L scale generation processes, we obtain the overall time complexity:

$$\sum_{l=1}^L \left(\frac{a^{2l} - 1}{a^2 - 1}\right)^2 = \frac{1}{(a^2 - 1)^2} \left(\frac{a^4(N^2 a^4 - 1)}{a^4 - 1} + \frac{2a^2(Na - 1)}{a^2 - 1} + \frac{1}{2} \log a^N \right) \sim \mathcal{O}(N^2). \quad (11)$$

For our MVAR method, at the l -th autoregressive generation stage, the total number of tokens is $N_l = a^{2(l-1)}$. Therefore, the time complexity for this stage is $\mathcal{O}(N_l k)$. Summing over all scales

yields:

$$\sum_{l=1}^L a^{2(l-1)} k = k \frac{a^{2L} - 1}{a^2 - 1} = k \frac{a^2 N - 1}{a^2 - 1} \sim \mathcal{O}(Nk). \quad (12)$$

C Additional Implementation Details of MVAR

We list the detailed training and sampling hyper-parameters for MVAR models in Table 5. For the predefined scale lengths inherited from VAR [46] (1, 2, 3, 4, 5, 6, 8, 10, 13, 16), we parallelize training across scales $r_1 \sim r_8$ to maximize GPU utilization, employing **diagonal-pattern** causal masks. This setup yields a uniform total token length of 256, which closely matches the token lengths of the final two scales (13×13 and 16×16).

Table 5: Detailed hyper-parameters for our MVAR models.

config	value
<i>training hyper-parameters</i>	
optimizer	AdamW [24]
base learning rate	1e-4
weight decay	0.05
optimizer momentum	(0.9, 0.95)
batch size	448 (d16) / 192 (d20) / 384 (d24)
total epochs	300 (train) / 80 (fine-tune)
warmup epochs	60 (train) / 2 (fine-tune)
precision	float16
max grad norm	2.0
dropout rate	0.1
class label dropout rate	0.1
params	310M (d16) / 600M (d20) / 1.0B (d24)
embed dim	1024 (d16) / 1280 (d20) / 1536 (d24)
attention head	16 (d16) / 20 (d20) / 24 (d24)
<i>sampling hyper-parameters</i>	
cfg guidance scale [19]	2.7 (d16) / 1.5 (d20) / 1.4 (d24)
top-k	1200 (d16) / 900 (d20) / 900 (d24)
top-p	0.99 (d16) / 0.96 (d20) / 0.96 (d24)

D Limitations and Future Work

In this work, we focus on the learning paradigm within the autoregressive transformer framework while retaining the original VQ-VAE architecture from VAR [46]. We anticipate that integrating more advanced image tokenizers [12, 22] could further enhance autoregressive visual generation performance. Future work may explore high-resolution image generation and video synthesis, which remain prohibitively expensive for traditional methods due to KV cache memory demands. Unlike conventional autoregressive models that rely on KV cache, our approach is inherently KV cache-free, reducing both memory consumption and computational complexity.

E More Qualitative Results

In Fig. 8, we show attention distributions of VAR alongside intermediate outputs at different scales. As the scale increases, the model progressively filters out irrelevant information from other scales and focuses attention on critical regions in adjacent scales.

In Fig. 9, we present generation results by our MVAR on ImageNet 256×256. Our MVAR generates high-quality images with notable diversity and fidelity.

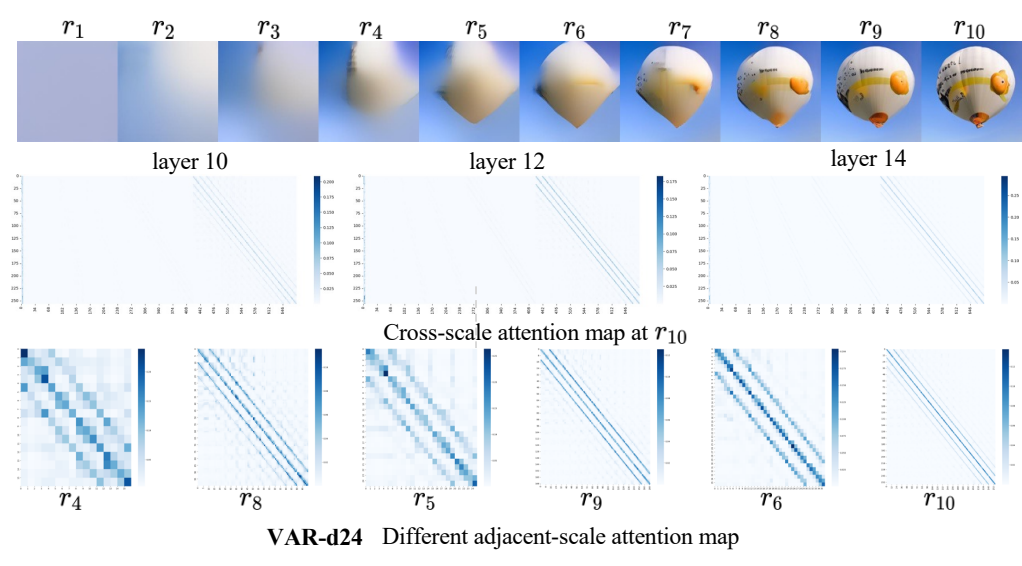
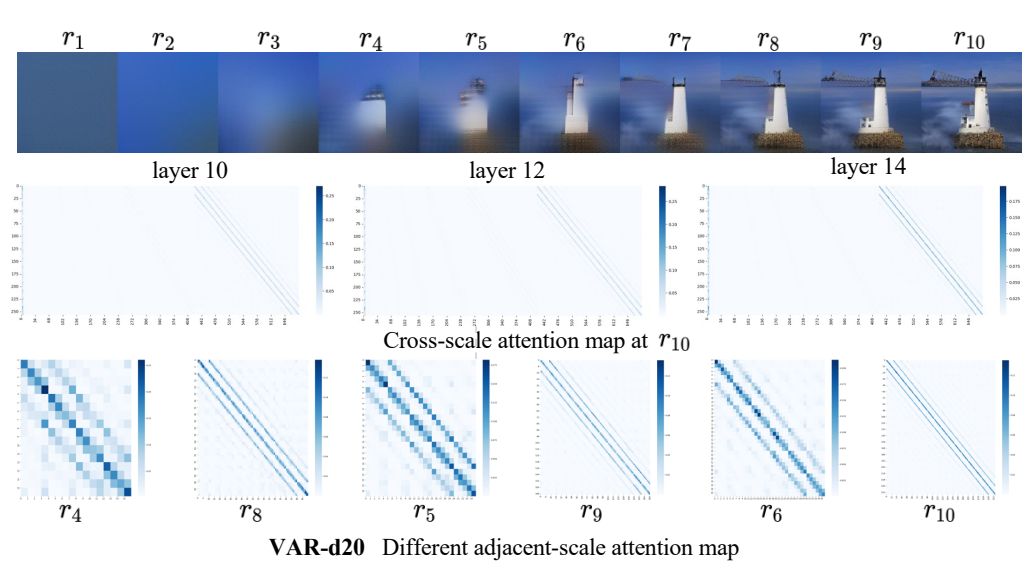
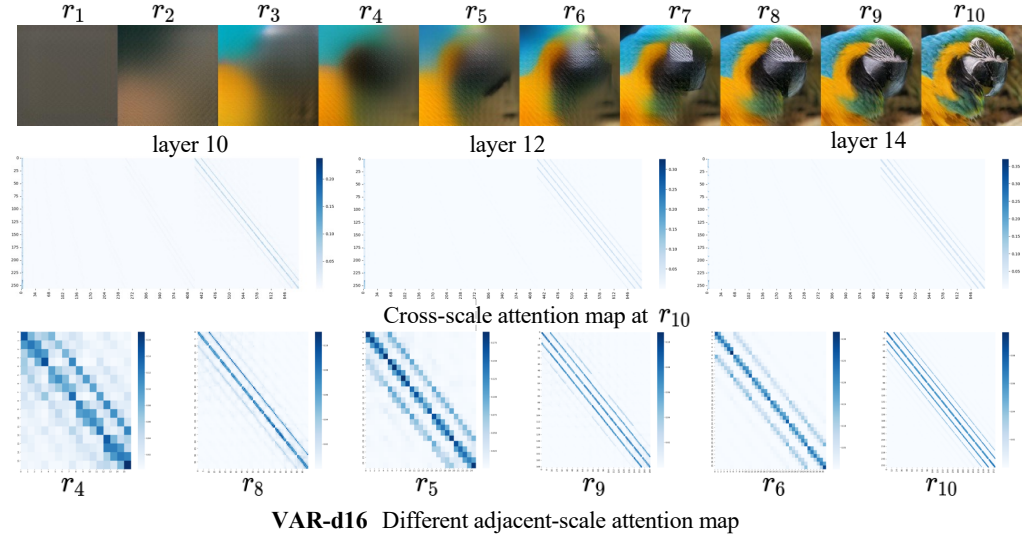


Figure 8: **Attention patterns in vanilla next-scale prediction (e.g., VAR).** Vanilla next-scale prediction exhibits redundant inter-scale dependencies and spatial redundancy.

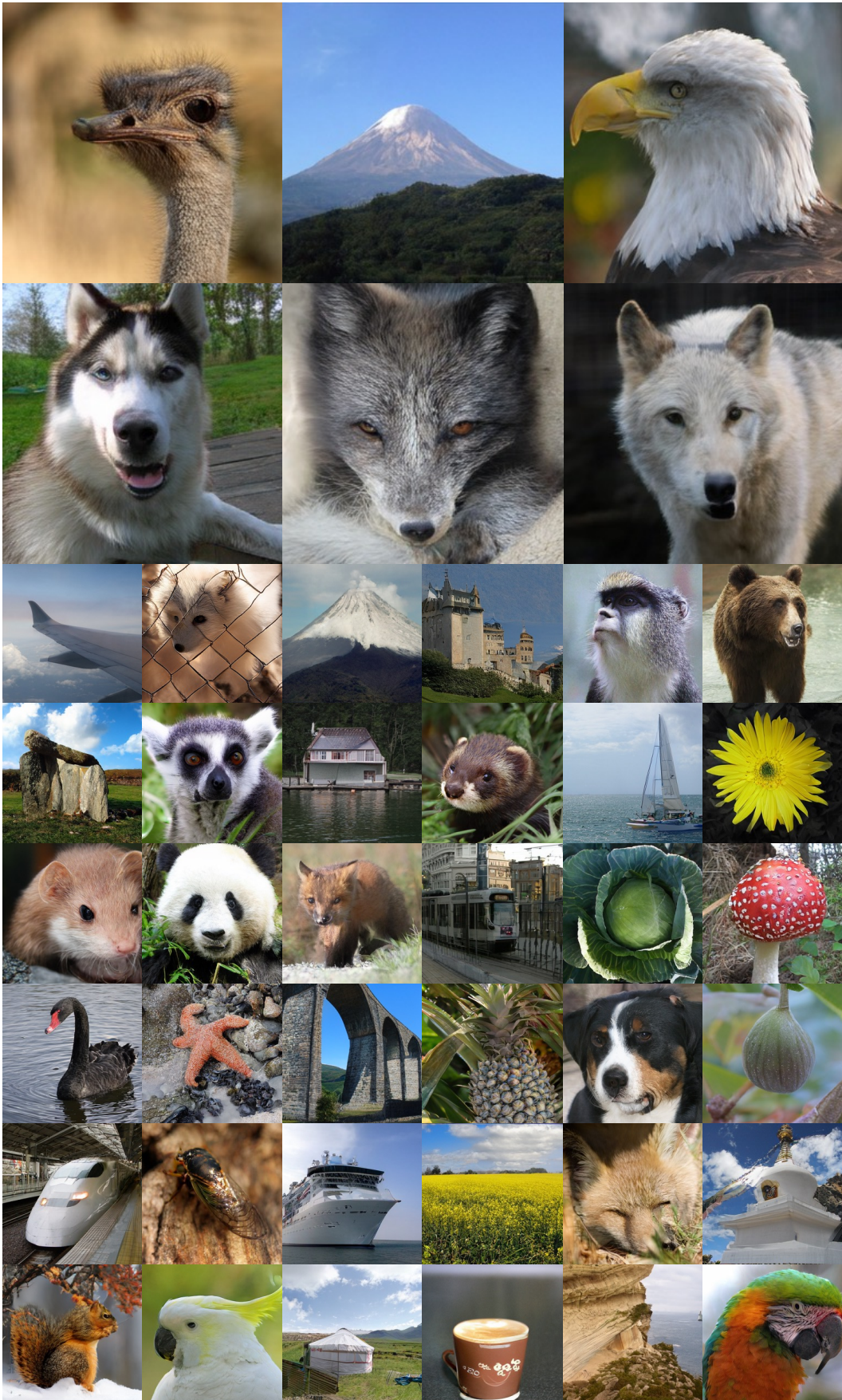


Figure 9: **Qualitative results.** Examples of class-conditional generation on ImageNet 256×256.

References

- [1] Brock, A., Donahue, J., Simonyan, K.: Large scale gan training for high fidelity natural image synthesis. arxiv 2018. arXiv preprint arXiv:1809.11096 (1809)
- [2] Chang, H., Zhang, H., Jiang, L., Liu, C., Freeman, W.T.: Maskgit: Masked generative image transformer. In: Proceedings of the IEEE/CVF conference on computer vision and pattern recognition. pp. 11315–11325 (2022)
- [3] Chen, R., Huang, W., Huang, B., Sun, F., Fang, B.: Reusing discriminators for encoding: Towards unsupervised image-to-image translation. In: Proceedings of the IEEE/CVF conference on computer vision and pattern recognition. pp. 8168–8177 (2020)
- [4] Chen, Z., Ma, X., Fang, G., Wang, X.: Collaborative decoding makes visual auto-regressive modeling efficient. arXiv preprint arXiv:2411.17787 (2024)
- [5] Denton, E.L., Chintala, S., Fergus, R., et al.: Deep generative image models using a laplacian pyramid of adversarial networks. Advances in neural information processing systems **28** (2015)
- [6] Dhariwal, P., Nichol, A.: Diffusion models beat gans on image synthesis. Advances in neural information processing systems **34**, 8780–8794 (2021)
- [7] Esser, P., Rombach, R., Ommer, B.: Taming transformers for high-resolution image synthesis. In: Proceedings of the IEEE/CVF conference on computer vision and pattern recognition. pp. 12873–12883 (2021)
- [8] Goodfellow, I., Pouget-Abadie, J., Mirza, M., Xu, B., Warde-Farley, D., Ozair, S., Courville, A., Bengio, Y.: Generative adversarial networks. Communications of the ACM **63**(11), 139–144 (2020)
- [9] Gu, J., Wang, Y., Zhang, Y., Zhang, Q., Zhang, D., Jaitly, N., Susskind, J., Zhai, S.: Dart: Denoising autoregressive transformer for scalable text-to-image generation. In: ICLR (2025)
- [10] Gu, S., Bao, J., Chen, D., Wen, F.: Giqa: Generated image quality assessment. In: Computer Vision–ECCV 2020: 16th European Conference, Glasgow, UK, August 23–28, 2020, Proceedings, Part XI 16. pp. 369–385. Springer (2020)
- [11] Guo, H., Li, Y., Zhang, T., Wang, J., Dai, T., Xia, S.T., Benini, L.: Fastvar: Linear visual autoregressive modeling via cached token pruning. arXiv preprint arXiv:2503.23367 (2025)
- [12] Han, J., Liu, J., Jiang, Y., Yan, B., Zhang, Y., Yuan, Z., Peng, B., Liu, X.: Infinity: Scaling bitwise autoregressive modeling for high-resolution image synthesis. arXiv preprint arXiv:2412.04431 (2024)
- [13] Hassani, A., Shi, H.: Dilated neighborhood attention transformer (2022), <https://arxiv.org/abs/2209.15001>
- [14] Hassani, A., Walton, S., Li, J., Li, S., Shi, H.: Neighborhood attention transformer. In: Proceedings of the IEEE/CVF Conference on Computer Vision and Pattern Recognition (CVPR). pp. 6185–6194 (June 2023)
- [15] He, K., Zhang, X., Ren, S., Sun, J.: Deep residual learning for image recognition. In: Proceedings of the IEEE conference on computer vision and pattern recognition. pp. 770–778 (2016)
- [16] Heusel, M., Ramsauer, H., Unterthiner, T., Nessler, B., Hochreiter, S.: Gans trained by a two time-scale update rule converge to a local nash equilibrium. Advances in neural information processing systems **30** (2017)
- [17] Ho, J., Jain, A., Abbeel, P.: Denoising diffusion probabilistic models. Advances in neural information processing systems **33**, 6840–6851 (2020)
- [18] Ho, J., Saharia, C., Chan, W., Fleet, D.J., Norouzi, M., Salimans, T.: Cascaded diffusion models for high fidelity image generation. Journal of Machine Learning Research **23**(47), 1–33 (2022)

- [19] Ho, J., Salimans, T.: Classifier-free diffusion guidance. arXiv preprint arXiv:2207.12598 (2022)
- [20] Hoogeboom, E., Heek, J., Salimans, T.: simple diffusion: End-to-end diffusion for high resolution images. In: ICML (2023)
- [21] Huang, Z., Qiu, X., Ma, Y., Zhou, Y., Zhang, C., Li, X.: Nfig: Autoregressive image generation with next-frequency prediction. arXiv preprint arXiv:2503.07076 (2025)
- [22] Jiao, S., Zhang, G., Qian, Y., Huang, J., Zhao, Y., Shi, H., Ma, L., Wei, Y., Jie, Z.: Flexvar: Flexible visual autoregressive modeling without residual prediction. arXiv preprint arXiv:2502.20313 (2025)
- [23] Kang, M., Zhu, J.Y., Zhang, R., Park, J., Shechtman, E., Paris, S., Park, T.: Scaling up gans for text-to-image synthesis. In: Proceedings of the IEEE/CVF Conference on Computer Vision and Pattern Recognition. pp. 10124–10134 (2023)
- [24] Kingma, D.P., Ba, J.: Adam: A method for stochastic optimization. arXiv preprint arXiv:1412.6980 (2014)
- [25] Lee, D., Kim, C., Kim, S., Cho, M., Han, W.S.: Autoregressive image generation using residual quantization. In: CVPR. pp. 11523–11532 (2022)
- [26] Li, T., Katabi, D., He, K.: Return of unconditional generation: A self-supervised representation generation method. In: The Thirty-eighth Annual Conference on Neural Information Processing Systems (2024)
- [27] Li, T., Tian, Y., Li, H., Deng, M., He, K.: Autoregressive image generation without vector quantization. arXiv preprint arXiv:2406.11838 (2024)
- [28] Liu, S., De Mello, S., Kautz, J.: Cosae: Learnable fourier series for image restoration. Advances in Neural Information Processing Systems **37**, 10236–10273 (2024)
- [29] Lu, C., Zhou, Y., Bao, F., Chen, J., Li, C., Zhu, J.: Dpm-solver: A fast ode solver for diffusion probabilistic model sampling in around 10 steps. Advances in Neural Information Processing Systems **35**, 5775–5787 (2022)
- [30] Van den Oord, A., Kalchbrenner, N., Espeholt, L., Vinyals, O., Graves, A., et al.: Conditional image generation with pixelcnn decoders. Advances in neural information processing systems **29** (2016)
- [31] Pang, Y., Jin, P., Yang, S., Lin, B., Zhu, B., Tang, Z., Chen, L., Tay, F.E., Lim, S.N., Yang, H., et al.: Next patch prediction for autoregressive visual generation. arXiv preprint arXiv:2412.15321 (2024)
- [32] Peebles, W., Xie, S.: Scalable diffusion models with transformers. In: Proceedings of the IEEE/CVF international conference on computer vision. pp. 4195–4205 (2023)
- [33] Peebles, W., Xie, S.: Scalable diffusion models with transformers. In: Proceedings of the IEEE/CVF International Conference on Computer Vision. pp. 4195–4205 (2023)
- [34] Peng, Y., Qi, J.: Cm-gans: Cross-modal generative adversarial networks for common representation learning. ACM Transactions on Multimedia Computing, Communications, and Applications (TOMM) **15**(1), 1–24 (2019)
- [35] Radford, A., Wu, J., Child, R., Luan, D., Amodei, D., Sutskever, I., et al.: Language models are unsupervised multitask learners. OpenAI blog **1**(8), 9 (2019)
- [36] Ramesh, A., Pavlov, M., Goh, G., Gray, S., Voss, C., Radford, A., Chen, M., Sutskever, I.: Zero-shot text-to-image generation. In: International conference on machine learning. pp. 8821–8831. Pmlr (2021)
- [37] Razavi, A., Van Den Oord, A., Vinyals, O.: Generating diverse high-fidelity images with vq-vae-2 (2019)

- [38] Rombach, R., Blattmann, A., Lorenz, D., Esser, P., Ommer, B.: High-resolution image synthesis with latent diffusion models. In: Proceedings of the IEEE/CVF conference on computer vision and pattern recognition. pp. 10684–10695 (2022)
- [39] Rombach, R., Blattmann, A., Lorenz, D., Esser, P., Ommer, B.: High-resolution image synthesis with latent diffusion models. In: Proceedings of the IEEE/CVF conference on computer vision and pattern recognition. pp. 10684–10695 (2022)
- [40] Salimans, T., Goodfellow, I., Zaremba, W., Cheung, V., Radford, A., Chen, X.: Improved techniques for training gans **29** (2016)
- [41] Salimans, T., Ho, J.: Progressive distillation for fast sampling of diffusion models. arXiv preprint arXiv:2202.00512 (2022)
- [42] Sauer, A., Schwarz, K., Geiger, A.: Stylegan-xl: Scaling stylegan to large diverse datasets. vol. abs/2201.00273 (2022), <https://arxiv.org/abs/2201.00273>
- [43] Song, J., Meng, C., Ermon, S.: Denoising diffusion implicit models. arXiv preprint arXiv:2010.02502 (2020)
- [44] Sun, P., Jiang, Y., Chen, S., Zhang, S., Peng, B., Luo, P., Yuan, Z.: Autoregressive model beats diffusion: Llama for scalable image generation. arXiv preprint arXiv:2406.06525 (2024)
- [45] Tang, H., Wu, Y., Yang, S., Xie, E., Chen, J., Chen, J., Zhang, Z., Cai, H., Lu, Y., Han, S.: HART: Efficient visual generation with hybrid autoregressive transformer. arXiv preprint arXiv:2410.10812 (2024)
- [46] Tian, K., Jiang, Y., Yuan, Z., Peng, B., Wang, L.: Visual autoregressive modeling: Scalable image generation via next-scale prediction. NeurIPS (2024)
- [47] Van Den Oord, A., Kalchbrenner, N., Kavukcuoglu, K.: Pixel recurrent neural networks. In: International conference on machine learning. pp. 1747–1756. PMLR (2016)
- [48] Van Den Oord, A., Vinyals, O., et al.: Neural discrete representation learning. NeurIPS **30** (2017)
- [49] Vaswani, A.: Attention is all you need. NeurIPS (2017)
- [50] Wang, X., Zhang, X., Luo, Z., Sun, Q., Cui, Y., Wang, J., Zhang, F., Wang, Y., Li, Z., Yu, Q., et al.: EMU3: Next-token prediction is all you need. arXiv preprint arXiv:2409.18869 (2024)
- [51] Xu, Y., Yin, Y., Jiang, L., Wu, Q., Zheng, C., Loy, C.C., Dai, B., Wu, W.: Transeditor: Transformer-based dual-space gan for highly controllable facial editing. In: Proceedings of the IEEE/CVF conference on computer vision and pattern recognition. pp. 7683–7692 (2022)
- [52] Yu, J., Li, X., Koh, J.Y., Zhang, H., Pang, R., Qin, J., Ku, A., Xu, Y., Baldridge, J., Wu, Y.: Vector-quantized image modeling with improved vqgan. arXiv preprint arXiv:2110.04627 (2021)
- [53] Yu, L., Cheng, Y., Sohn, K., Lezama, J., Zhang, H., Chang, H., Hauptmann, A.G., Yang, M.H., Hao, Y., Essa, I., et al.: Magvit: Masked generative video transformer. In: Proceedings of the IEEE/CVF Conference on Computer Vision and Pattern Recognition. pp. 10459–10469 (2023)